arXiv:1605.03397v1 [physics.comp-ph] 11 May 2016

Dry deposition model for a microscale aerosol dispersion solver based on the moment method

Viktor Šíp[a,*], Luděk Beneš[a]

[a]*Department of Technical Mathematics, Faculty of Mechanical Engineering, Czech Technical University in Prague. Karlovo náměstí 13, 121 35 Prague 2, Czech Republic.*

Abstract

A dry deposition model suitable for use in the moment method has been developed. Contributions from five main processes driving the deposition - Brownian diffusion, interception, impaction, turbulent impaction, and sedimentation - are included in the model. The deposition model was employed in the moment method solver implemented in the OpenFOAM framework. Applicability of the developed expression and the moment method solver was tested on two example problems of particle dispersion in the presence of a vegetation on small scales: a flow through a tree patch in 2D and a flow through a hedgerow in 3D. Comparison with the sectional method showed that the moment method using the developed deposition model is able to reproduce the shape of the particle size distribution well. The relative difference in terms of the third moment of the distribution was below 10% in both tested cases, and decreased away from the vegetation. Main source of this difference is a known overprediction of the impaction efficiency. When tested on the 3D test case, the moment method achieved approximately eightfold acceleration compared to the sectional method using 41 bins.

Keywords: Dry deposition, Vegetation, Microscale modeling, Moment method, Particle dispersion

1. Introduction

Urban vegetation is receiving a significant amount of attention from researchers in recent years. This interest stems from its impacts on the environment, affecting the pedestrian comfort and mitigating the negative health effects of the air pollution (Litschke and Kuttler, 2008; Janhäll, 2015).

Microscale modelling using the computational fluid dynamics (CFD) proved to be an indispensable tool for assessing the impacts of the vegetation in the

*Corresponding author
Email address: viktor.sip@fs.cvut.cz (Viktor Šíp)

urban settings. Some numerical studies focused only on the effects of the vegetation on the flow (Kenjereš and ter Kuile, 2013) or on the thermal comfort of the pedestrian (Mochida and Lun, 2008). Others investigated pollutant dispersion in the presence of the vegetation, but without taking the deposition of the pollutant into account (Jeanjean et al., 2015; Gromke and Blocken, 2015a,b). When including the deposition, authors opted both for simplified model with constant deposition velocity (Vranckx et al., 2015) and complex models expressing the dependence of the deposition velocity on various parameters such as the particle size or the wind speed (Tiwary et al., 2005; Steffens et al., 2012).

Dispersion of the particles with a fixed size can be described by one scalar partial differential equation. When the behaviour of the particle size distribution is of interest, straightforward approach - so called *sectional* approach - is to divide the size range into a number of discrete bins and then model the appropriate number of scalar PDEs, i.e. one for each bin. Other option is to use the transport equation for the moments of the particle size distribution. Such approach can reduce the number of PDEs to be solved, and therefore reduce the computational demands. This class of methods, here referred to as the *moment method*, has been used for the simulation of the aerosol behaviour for a long time (Whitby et al., 1991).

Usage of the moment method in the air quality models is also widespread (e.g. Binkowski and Shankar, 1995; Pirjola et al., 1999; Jung et al., 2003). Adapting the deposition velocity models to the moment method framework is not straightforward, since the mathematical formulation of the moment method requires all terms in the equation to be in the form of the power law of the particle size. Binkowski and Shankar (1995) simplified the problem by using the resistance model with Brownian particle diffusivity and settling velocity averaged over the particle size range. Bae et al. (2009) developed a deposition velocity model based on the model proposed by Raupach et al. (2001a). This model, however, only includes the processes of Brownian diffusion, impaction and gravitational settling, and does not take into account the processes of interception and turbulent impaction, which play an important role in the dry deposition process (Petroff et al., 2008b).

This study aims to fix this shortcoming by adapting the model by Petroff et al. (2008b) for the use in the moment method. The developed model is then used in the microscale CFD solver to solve the problems of a pollutant dispersion in the presence of a vegetation. To the authors' best knowledge, the moment method has not yet been applied to the microscale urban vegetation problems. Comparison of the obtained results with the results from the sectional model shows the applicability of such approach.

2. Mathematical formulation

2.1. Number concentration equation

The governing equation for the transport and the deposition of the aerosol particles of a diameter d_p in the flow field given by the velocity $\boldsymbol{u}$ can be for-

mulated as

$$\frac{\partial n(d_p)}{\partial t} = -\underbrace{\nabla \cdot \boldsymbol{u} n(d_p)}_{\text{Convection}} + \underbrace{\nabla \cdot D \nabla n(d_p)}_{\text{Diffusion}} - \underbrace{\nabla \cdot \boldsymbol{u}_s(d_p) n(d_p)}_{\text{Gravitational settling}} - \underbrace{\text{LAD} u_d(d_p) n(d_p)}_{\text{Deposition}}, \tag{1}$$

where $n(d_p)$ is the number concentration of the particles (Whitby and McMurry, 1997). Diffusion coefficient $D = \nu_T / Sc_T$ is expressed as a fraction of the turbulent viscosity and the turbulent Schmidt number. Effects of the gravitational acceleration $\boldsymbol{g}$ are captured in the terminal settling velocity of a particle, given by the Stokes' equation,

$$\boldsymbol{u}_s(d_p) = \frac{d_p^2 \rho_p \boldsymbol{g} C_C}{18\mu}, \tag{2}$$

where ρ_p is the density of the particle, μ is the dynamic viscosity of air, and C_C is the Cunningham correction factor (Hinds, 1999). The formula used for the correction factor is discussed in section 2.3.1.

The removal of the particles via dry deposition is modelled by a product of three parameters: *leaf area density* (LAD), defined as a leaf area per unit volume ($\mathrm{m}^2\ \mathrm{m}^{-3}$), deposition velocity u_d ($\mathrm{m\,s}^{-1}$) measuring the filtration efficiency of the vegetation under given conditions, and the particle concentration (Raupach et al., 2001b). Its form is discussed in section 2.3.

2.2. Moment equations

The moment method is based on the idea that in order to model the size distribution of the particles, we can investigate the behaviour of the moments of the distribution. Moment of the distribution is defined as

$$M_k = \int_0^\infty d_p^k n(d_p) \mathrm{d}d_p, \tag{3}$$

where k is the order of the moment. Some moments have straightforward physical interpretation: $M_0 = \int_0^\infty n(d_p)\mathrm{d}d_p = N$ is the total number concentration, $M_2 = \int_0^\infty d_p^2 n(d_p)\mathrm{d}d_p = 1/\pi \cdot S$ is proportionate to the surface area concentration and $M_3 = \int_0^\infty d_p^3 n(d_p)\mathrm{d}d_p = 6/\pi \cdot V$ is proportionate to the volume concentration.

Assuming $n(d_p)$ is sufficiently smooth in space and time, moment equations are obtained by multiplying Eq. (1) by d_p^k, integrating over the whole size range and interchanging the derivatives and the integrals:

$$\begin{aligned} \frac{\partial M_k}{\partial t} = &- \underbrace{\nabla \cdot \boldsymbol{u} M_k}_{\text{Convection}} + \underbrace{\nabla \cdot D \nabla M_k}_{\text{Diffusion}} - \underbrace{\int_0^\infty d_p^k \nabla \cdot \boldsymbol{u}_s(d_p) n(d_p) \mathrm{d}d_p}_{\text{Gravitational settling}} \\ &- \underbrace{\text{LAD} \int_0^\infty d_p^k u_d(d_p) n(d_p) \mathrm{d}d_p}_{\text{Deposition}}. \end{aligned} \tag{4}$$

Now we are left with the evaluation of the integrals in (4). This can be done easily if the multiplicative terms are in a form of a polynomial function of d_p. Such is the case with the gravitational term, if we take into account that gravity plays significant role only for larger particles, where the Cunningham correction factor C_C in (2) can be left out. Using (2) in the third term on the RHS of (4), the term can be rewritten as

$$-\nabla \cdot \boldsymbol{g} \frac{\rho_p}{18\mu} \int_0^\infty d_p^{k+2} n(d_p) \mathrm{d}d_p = -\nabla \cdot \boldsymbol{g} \frac{\rho_p}{18\mu} M_{k+2}. \tag{5}$$

Here we introduced a dependence on the moment of a higher order. That necessitates that we either solve a separate moment equation also for this higher order moment, or that this moment can be calculated from the moments that we solve for.

The task of integrating the deposition term is more difficult and will be examined in the following section.

2.3. Deposition model for the moment method

Variety of models describing the rate of particle transport from the air to the vegetation surface has been proposed (Petroff et al., 2008a). Dry deposition schemes used in the large-scale air quality models are usually formulated in terms of a friction velocity or a wind speed at some height above the canopy, and do not explicitely model the behaviour inside the canopy. As such, they are not directly applicable in the microscale CFD models, but the same principles governing the deposition still apply.

In this study we adopted the deposition velocity expression given by Petroff et al. (2008b) for needle-like obstacles. Petroff et al. (2008b) formulated the expressions for deposition velocities (or collection velocities in the original terminology) associated with each of the five main processes driving the dry deposition inside the canopy. The model then assumes that these processes, which are the Brownian diffusion, interception, impaction, turbulent impaction, and sedimentation, are acting in parallel and independently. The deposition velocity thus can be written as a sum of the deposition velocities of all processes,

$$u_d = u_{BD} + u_{IN} + u_{IM} + u_{TI} + u_{SE}. \tag{6}$$

Contributions of each process to the deposition velocity for an exemplary set of parameters are shown on Fig. 1.

The assumption of the parallel and independent acting is advantageous for adapting the model to the moment method, since it allows us to split the rightmost integral in Eq. (4) into integrals pertaining to the every physical process separately. In this section, we will describe each process in more detail and show how it can be adapted to the moment method.

Few simplifications were made to the original model to make the subsequent analysis simpler: we considered only plagiophile canopies and Dirac distribution of the needle sizes. Also note that here we focus only on needle-like obstacles. Similar model for broadleaf canopies, given in (Petroff et al., 2009), could be adapted to the moment method as well.

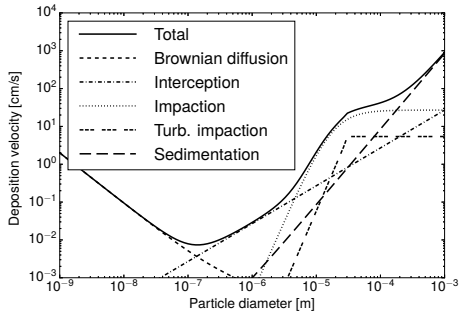

Figure 1: Dependence of the deposition velocity on the particle diameter in the original model ($\rho_p = 1300\,\mathrm{kg\ m^{-3}}, d_e = 2\,\mathrm{mm}, U = 1\,\mathrm{m\,s^{-1}}, u_f = 0.3\,\mathrm{m\,s^{-1}}$. See sections 2.3.1 - 2.3.5 for the description of the parameters).

2.3.1. Brownian diffusion

Brownian diffusion is the dominant process driving the deposition of the particles smaller then 0.1 µm (Litschke and Kuttler, 2008). Original model formulates the contribution to the deposition velocity due to the Brownian diffusion as

$$u_{BD} = UC_B Sc^{-2/3} Re^{n_B - 1} \tag{7}$$

where U is the magnitude of the wind velocity, $Sc = \nu_a / D_B$ is the Schmidt number (with ν_a being the kinematic viscosity of air and D_B the Brownian diffusion coefficient, $D_B = (C_C k_b T_a)/(3\pi\mu_a d_p))$, $Re = U d_e / \nu_a$ is the Reynolds number, and d_e is the needle diameter. Assuming laminar boundary layer around the obstacles, the model constants hold the values $n_B = 0.5$ and $C_B = 0.467$.

Cunningham correction factor $C_C^A = 1 + 2\lambda/d_p(1.257 + 0.4\exp(-1.1 d_p/2\lambda))$ is used in the original model (Petroff et al., 2008b), where λ is the mean free path of the particle in the air. In this whole study we use simpler approximation $C_C^B = 1 + 3.34\lambda/d_p$ (Bae et al., 2009). Comparison of these expressions is on Fig. 2, where it can be seen that their difference peaks to 12% for particle diameter around 0.2 µm.

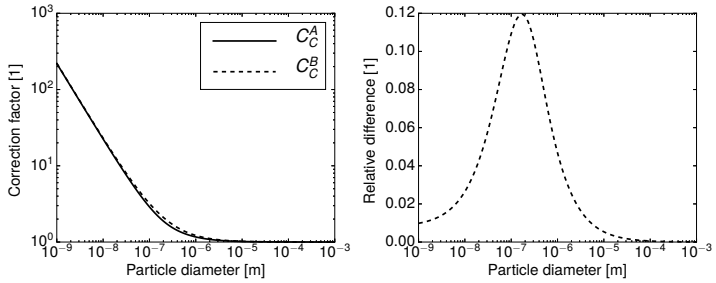

Figure 2: (Left) Two expressions for the Cunningham correction factor. (Right) Relative difference $(C_C^B - C_C^A)/C_C^A$.

Furthermore, for the Brownian diffusion we take into account only the size-dependent part of the correction factor, dominant in the particle size range where the diffusion is significant, $C_C \approx 3.34\frac{\lambda}{d_p}$. Putting the expressions above into Eq. (7), we obtain

$$u_{BD} \approx u'_{BD} = U^{n_B}\gamma_1\gamma_2^{2/3}d_p^{-4/3}, \tag{8}$$

where $\gamma_1 = C_B\left(d_e/\nu_a\right)^{n_B-1}\left(3\pi\nu_a^2\rho_a/(k_bT_a)\right)^{-2/3}$ and $\gamma_2 = 3.34\lambda$.

Using this formula, the contribution to the moment equation can be written as

$$\left.\frac{\partial M_k}{\partial t}\right|_{BD} = -\mathrm{LAD}\ U^{n_B}\gamma_1\gamma_2^{2/3}M_{k-4/3}. \tag{9}$$

2.3.2. Interception

Interception denotes the process where the particle follows the streamline, but too close to the obstacle so that it is captured on the surface. The original model parameterizes its contribution to the deposition velocity as

$$u_{IN} = 2Uk_x\frac{d_p}{d_e}, \tag{10}$$

where $k_x = 0.27$ is the ratio of the leaf surface projected on the plane perpendicular to the flow to the total leaf surface.

Since there is a linear dependence on the particle diameter, the expression can be integrated as is, resulting in

$$\left.\frac{\partial M_k}{\partial t}\right|_{IN} = -\mathrm{LAD}\gamma_3 U M_{k+1}, \tag{11}$$

with $\gamma_3 = 2k_x/d_e$.

2.3.3. Inertial impaction

Inertial impaction occurs when particles do not follow the streamlines due to their inertia, resulting in the collision with the obstacle. The deposition velocity due to the inertial impaction is written as

$$u_{IM} = Uk_xE_{IM}, \tag{12}$$

where $E_{IM} = \left(\frac{St}{St+\beta}\right)^2$ is the impaction efficiency with the constant $\beta = 0.6$. To use this deposition velocity in the moment equations, we approximate the impaction efficiency as $E'_{IM} = \min(a\ St^b, 1)$, where the coefficients $a = 0.407$ and $b = 1.039$ were obtained by minimizing the quadratic error of the original function and the approximation for $St \in [0, 1]$. The original function and the approximation are shown on Fig. 3. It is clear that this approximation introduces overprediction of the impaction efficiency for Stokes numbers between 1 and 10. This was however deemed to be an acceptable compromise between the accuracy and the computational efficiency. Without the approximation, one could

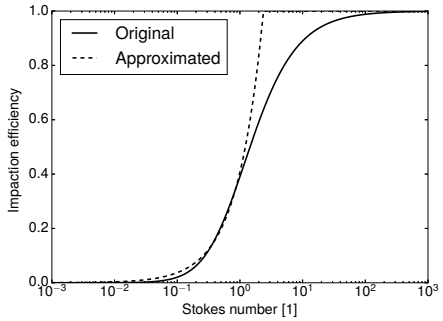

Figure 3: Original and approximated expressions for the impaction efficiency.

use the numerical integration to evaluate the integral to obtain more precise approximation of the original formula, but at a significantly higher computational cost.

Approximated deposition velocity can then be formally written as

$$u'_{IM} = Uk_x E'_{IM}. \tag{13}$$

After some algebraic manipulations the corresponding term in the moment equation can be written using the incomplete moments $M_k^-(x) = \int_0^x d_p^k n(d_p) \mathrm{d}d_p$ and $M_k^+(x) = \int_x^\infty d_p^k n(d_p) \mathrm{d}d_p$ as

$$\left.\frac{\partial M_k}{\partial t}\right|_{IM} = -\mathrm{LAD}\ Uk_x \left(U^b \gamma_4 M^-_{k+2b}(d_p^{T1}) + M_k^+(d_p^{T1})\right) \tag{14}$$

with the threshold $d_p^{T1} = \sqrt{\frac{18\mu_a d_c}{\rho_p U a^{1/b}}}$ and $\gamma_4 = a\left(\frac{\rho_p}{18\mu_a d_e}\right)^b$.

2.3.4. Turbulent impaction

Effect of the particle impaction due to the canopy turbulence is described by the deposition velocity

$$u_{TI} = \begin{cases} u_f K_{TI1} {\tau_p^+}^2 & \text{if } \tau_p^+ < 20, \\ u_f K_{TI2} & \text{if } \tau_p^+ \geq 20. \end{cases} \tag{15}$$

Here $\tau_p^+ = \tau_p u_f^2/\nu_a$ is the dimensionless particle relaxation time, $\tau_p = \frac{\rho_p C_c d_p^2}{18\mu_a}$ is the particle relaxation time, u_f is the local friction velocity, $K_{TI1} = 3.5 \cdot 10^{-4}$, and $K_{TI2} = 0.18$. The contribution to the moment equation can be again expressed using the incomplete moments,

$$\left.\frac{\partial M_k}{\partial t}\right|_{TI} = -\mathrm{LAD}\left(u_f^5 \gamma_5 M^-_{k+4}(d_p^{T2}) + u_f K_{TI2} M_k^+(d_p^{T2})\right) \tag{16}$$

with the threshold $d_p^{T2} = \sqrt{\frac{360\mu_a\nu_a}{\rho_p u_f^2}}$ and $\gamma_5 = \frac{K_{TI1}\rho_p^2\rho_a^2}{(18\mu_a^2)^2}$.

2.3.5. Sedimentation

Sedimentation plays the major role for the particles with the diameter above 10 µm. The sedimentation contribution to the deposition velocity is expressed as

$$u_{SE} = \frac{k_z g \rho_p C_C d_p^2}{18 \mu_a}, \tag{17}$$

where $k_z = 0.22$ is the ratio of the leaf surface projected to the horizontal plane to the total leaf surface.

Substituting this expression to the integral in the moment equation, after some algebraic manipulations we obtain

$$\left.\frac{\partial M_k}{\partial t}\right|_{SE} = -\mathrm{LAD}\gamma_6(M_{k+2} + \gamma_2 M_{k+1}) \tag{18}$$

with $\gamma_6 = \frac{k_z g \rho_p}{18 \mu_a}$ and $\gamma_2 = 3.34\lambda$ as before.

2.3.6. Comparison with the original model

The developed model can be formally written as

$$u_d = u'_B + u_{IN} + u'_{IM} + u_{TI} + u_{SE} \tag{19}$$

using the Equations (8), (10), (13), (15) and (17). In the moment method solver it is however implemented via the Equations (9), (11), (14), (16) and (18). Two major approximation were made: first, Cunningham approximation factor is replaced by its size-dependent part in the Brownian diffusion term. Secondly, an inexact power law formula is used for the impaction efficiency.

Comparison of this model with the original for an exemplary set of parameters is shown on Fig. 4. The higher values of the deposition velocity for particles around 3 µm are the consequence of the inexact approximation to the inertial impaction term described in section 2.3.3.

The maximal difference of the deposition velocity given by the two models was determined by evaluating the deposition velocity for every combination of the parameters in the ranges expected in real-world situations ($\rho_p \in [500; 3000]$ kg m^{-3}, $d_e \in [0.5; 5]$ mm, $U \in [0, 10]$ m s^{-1}, $d_p \in [10^{-3}, 10^2]$ µm). Each interval was discretized using 50 points. Local friction velocity u_f was set to 0 m s^{-1}, as the turbulent impaction is implemented exactly and its contribution can only reduce the relative difference of the deposition velocities. The largest relative difference $|u_d^{orig} - u_d^{approx}|/\min(u_d^{orig}, u_d^{approx})$ was found to be 4.56 for the parameter values at the end of the expected ranges ($\rho_p = 3000$ kg m^{-3}, $d_e = 5$ mm, $U = 10$ m s^{-1}) and particle diameter $d_p = 5.67$ µm, giving the deposition velocities $u_d^{orig} = 0.106$ cm s^{-1} and $u_d^{approx} = 0.591$ cm s^{-1}.

While this difference is certainly significant, measured values shows even higher variability (Litschke and Kuttler, 2008). Considering this, the costs of the alternative to this approximation - i.e. the numerical integration of the impaction term integral - does not outweigh the better fit to the original model.

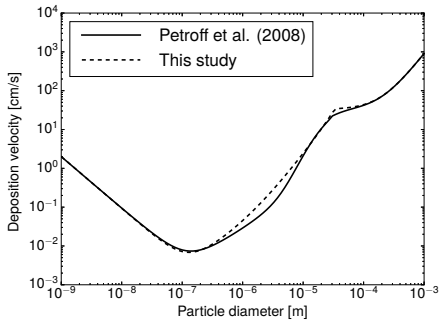

Figure 4: Comparison of the deposition velocities given by the original model and the one developed in this study ($\rho_p = 1300\,\mathrm{kg\ m^{-3}}, d_e = 2\,\mathrm{mm}, U = 1\,\mathrm{m\,s^{-1}}, u_f = 0.3\,\mathrm{m\,s^{-1}}$).

2.4. Lognormal distribution

Before we move on to the description of the implementation, it is necessary to provide some assumptions on the particle size distribution. Size distributions of the atmospheric aerosols are often well fitted by a multimodal lognormal distribution (Seinfeld and Pandis, 2006). This is the distribution we will use from now on. We restrict ourselves only to the case of unimodal distribution, noting that the multimodal distribution can be modelled by a superposition of several unimodal distributions.

Unimodal lognormal distribution can be described by three parameters: total number concentration N, geometric mean size d_{gn} and geometric standard deviation σ_g. Its probability density function is

$$n(\ln d_p) = \frac{N}{\sqrt{2\pi}\ln\sigma_g}\exp\left(-\frac{(\ln d_p - \ln d_{gn})^2}{2\ln^2\sigma_g}\right). \tag{20}$$

Knowing the three parameters, k-th moment can be calculated using the formula

$$M_k = N d_{gn}^k \exp\left(\frac{k^2}{2}\ln^2\sigma_g\right). \tag{21}$$

From the three moments of order 0, k_1 and k_2 the three parameters can be obtained using the relations

$$N = M_0, \tag{22}$$

$$d_{gn} = \overline{M}_{k_1}^{\frac{1}{r(k_2-k_1)}}\,\overline{M}_{k_2}^{\frac{r}{k_1-k_2}}, \tag{23}$$

$$\ln^2\sigma_g = \frac{2}{k_1(k_1-k_2)}\ln\left(\frac{\overline{M}_{k_1}}{\overline{M}_{k_2}^{r}}\right), \tag{24}$$

where $\overline{M}_k = \frac{M_k}{M_0}$ and $r = \frac{k_1}{k_2}$ (Whitby and McMurry, 1997).

For the incomplete higher order moments following holds:

$$M_k^-(x) = \int_0^x d_p^k n(d_p) \mathrm{d}d_p = M_k \Phi \left(\frac{\ln x - \ln d_{gn} - k \ln^2 \sigma_g}{\ln \sigma_g} \right), \tag{25}$$

$$M_k^+(x) = \int_x^\infty d_p^k n(d_p) \mathrm{d}d_p = M_k \left(1 - \Phi \left(\frac{\ln x - \ln d_{gn} - k \ln^2 \sigma_g}{\ln \sigma_g} \right) \right), \tag{26}$$

where Φ is the normal cumulative distribution function.

2.5. Choice of the moments

Now we turn our attention to the choice of the moments. For which orders we decide to solve the moment equation (4) is to a degree an arbitrary decision. When this problem is discussed in literature, cited reasons for a certain choice include the mathematical simplicity and ease of the formulation of the modelled processes or the physical interpretation of some moments (Whitby and McMurry, 1997; Binkowski and Shankar, 1995). Choices of the moments used in the field of atmospheric aerosol modelling in the selected literature are summarized in Tab. 1.

Reference	Moments
(Binkowski and Shankar, 1995)	0, 3, 6
(Pirjola et al., 1999)	0, 2, 3
(Jung et al., 2003)	0, 2, 3
(Koziol and Leighton, 2007)	0, 1, 2
(Bae et al., 2009)	0, 3, 6

Table 1: Choices of the moments in the selected literature

The recurrent usage of zeroth order moment brings substantial advantage, as it is equal to the total number concentration, and it is the order we will use as well. On the choice of the other moments authors differ.

To assess the influence of the choice of the moments, following numerical experiment was performed. We investigated the particle deposition in a 1D tube, spanning between 0 and 300 m. Homogenous vegetation block of LAD = 3 $\mathrm{m}^2\ \mathrm{m}^{-3}$ was placed between 100 a 150 m. Velocity of the air in the whole tube was set to constant 1 $\mathrm{m\,s}^{-1}$, unaffected by the vegetation. Source of the pollutant was placed at 50 m from the inlet with the intensity of number of particles 1 s^{-1} and the distribution parameters $\sigma_g = 0.7, d_{gn} = 3\mu\mathrm{m}$. The tube was discretized using 400 cells.

Beside the choices mentioned in Tab. 1, we tested also a variant with a negative order moment: 0, -1, 1. Non integer choices of the orders would also be possible to use, but we saw no advantage that such choice could bring.

Transport and the deposition of the pollutant was calculated by the sectional model based on the Eq. (1) and by the moment method based on the Eq. (4) (see section 2.6 for details on the implementation). To discard possible errors due to the inexact approximation of the deposition velocity, only

the sedimentation contribution, adapted exactly, was taken into account. The numerical experiment is not meant to model any real-world situation, rather just demonstrate the behaviour of the moment method in a simple setting.

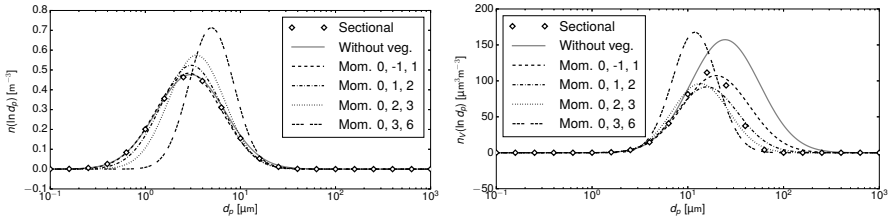

Figure 5: (Left) Number concentration (Right) Volume concentration

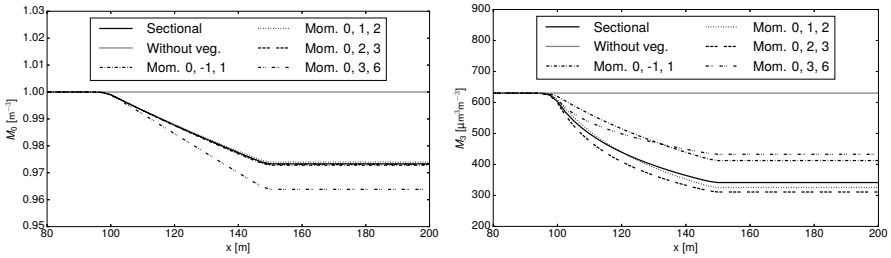

Figure 6: Evolution of the moments along 1-dimensional the tube. (Left) Zeroth moment (Right) Third moment.

Number and volume concentration distribution behind the barrier (at 150 m) are shown on Fig. 5. As a reference, calculated distributions are complemented by the distribution for a case without the vegetation present. Evolution of the zeroth moment (equal to the number concentration) and the third moment (proportional to the volume concentration) through the vegetation block are shown on Fig. 6.

Effect of the vegetation, while small in number concentration, is significant in volume concentration. Only the variant using the moments of orders 0, -1, and 1 reproduces well the number concentration distribution, but overpredicts the peak of the volume concentration. Variants using the orders 0, 1, 2 and 0, 2, 3 produce result closer to the sectional model in volume concentration, but with larger differences in number concentration. Variant using the orders 0, 3, 6 shows no advantages over the other variants.

Choosing between the orders 0, 1, 2 and 0, 2, 3, we opted for the latter variant, as the third moment is proportionate to the main quantity of interest - volume (and mass) concentration of the pollutant.

2.6. Numerical implementation

Both the sectional model and the moment model were implemented using the OpenFOAM platform (Greenshields, 2015). Second order upwind scheme

was used for convective terms in Equations (1) and (4) and second order scheme based on the Gauss theorem was used for the diffusive terms. Residual levels of 10^{-5} were used to test for convergence of the steady state solver.

When using the moment method, we have to solve the discretized Eq. (4) for the three selected moments. These equations are coupled through the gravitational settling term and the deposition term, which depends on the moments of a different order than the one solved by the equation. The coupling is dealt with the following way. In every iteration, first the parameters of the lognormal distribution N, d_{gn} and σ_g are calculated using the Equations (22-24) from the values in the preceeding iteration. Three moment equations are then solved one after another with the coupling terms resulting from the deposition being treated explicitly.

Fully explicit treatment of the gravitational settling term (5) can result in numerical instability, unless low values of the relaxation factors are used. That would however lead to slower convergence, therefore we employed a semi-implicit treatment. Moment M_{k+2} in (5) is rewritten as $M_{k+2} = F_{k,2}M_k$ with

$$F_{k,m} = M_{k+m}/M_k = d_{gn}^m \exp\left(\frac{m(m+2k)}{2}\ln^2\sigma_g\right) \tag{27}$$

and the term $F_{k,2}$ is then treated explicitly and M_k implicitly.

Relaxation factors 0.95 were used both for the sectional equations and for the moment equations. For the first five iterations of the moment method the relaxation factors for the moment equations were however set to lower value 0.8, as the computations proved to be less stable at the beginning.

Calculation of the distribution parameters d_{gn} and $\ln^2\sigma_g$ via Eq. (23) and (24) includes the division of the moments, potentially very small far away from the source of pollutant. To avoid this problem, small background concentration in the whole domain is set as an initial condition and used as a boundary condition where zero would be used otherwise.

3. Applications

Here we describe two example problems of microscale flows through and around the vegetation and assess the applicability of the developed moment method to the simulation of pollutant dispersion. Two vegetation elements that could be encountered in the urban settings are investigated in this test: small patch of full grown trees and a dense hedgerow.

The flow field in both cases was precomputed by an in-house finite volume CFD solver. The solver is based on the Navier-Stokes equations in the Boussinesq approximation and utilizes $k-\epsilon$ turbulence model. Inlet profiles of velocity and the turbulence quantities, as well as the wall functions, are prescribed by the analytical expressions given by Richards and Hoxey (1993). Vegetation model for the momentum and $k-\epsilon$ equations described by Katul et al. (2004) is employed. For further details we refer to (Šíp and Beneš, 2016), where the solver

is described in more detail. Turbulent Schmidt number was set to $Sc_T = 0.7$ in both cases, based on the analysis by Tominaga and Stathopoulos (2007).

In both cases presented below, we simulated the dispersion of a coarse mode particles from a point or a line source. The coarse mode is chosen as the mode that contains, together with the accumulation mode, majority of the volume of the particles in the urban environment (Seinfeld and Pandis, 2006), but is affected more strongly by the dry deposition than the accumulation mode. The number distribution at the source is assumed to be lognormal with the parameters $d_{gn} = 0.86$µm and $\sigma_g = 2.21$, typical for the urban environment (Hinds, 1999).

Evaluation of the developed moment method was based on the comparison with the results obtained by the sectional model. In the sectional model, Eq. (1) is solved for 41 particle sizes distributed uniformly between 0.01 µm and 100 µm. The interval is chosen so that the behaviour of the number distribution as well as the volume distribution can be captured by the sectional model.

3.1. Tree patch in 2D

First case investigates the filtering properties of a small patch of full grown conifer trees. A simplified 2D model is constructed as follows. The 30 meters wide and 15 meters high tree patch is represented as a horizontally homogeneous vegetation block. Pollutant source is placed 15 meters upstream from the vegetation, 5 meters above the ground. LAD profile of the vegetation is prescribed

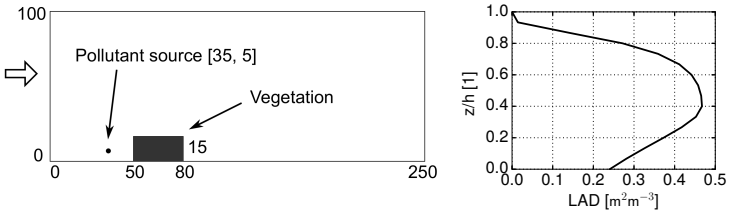

Figure 7: (Left) Sketch of the domain. All dimensions in meters. Sketch is not to scale. (Right) LAD profile of the vegetation.

by a formula given by Lalic and Mihailovic (2004),

$$\mathrm{LAD}(z) = L_m \left(\frac{h - z_m}{h - z}\right)^n \exp\left(n\left(1 - \frac{h - z_m}{h - z}\right)\right), \tag{28}$$

$$n = \begin{cases} 6 & \text{if } 0 \le z < z_m, \\ 0.5 & \text{if } z_m \le< z \le h, \end{cases}$$

where $h = 15$ m is the height of the trees, L_m is the maximum LAD, chosen so that leaf area index, $\mathrm{LAI} = \int_0^h \mathrm{LAD}(z)\mathrm{d}z$, is equal to 5, and $z_m = 0.4h$ is the corresponding height of maximal LAD. The sketch of the domain and the LAD profile of the vegetation is shown on Fig. 7. Trees are modelled as generic

conifers with $d_e = 2\,\mathrm{mm}$. The drag coefficient is chosen as $C_d = 0.3$ (Katul et al., 2004).

Intensity of the point source is set to a normalized value $1\,\mathrm{s}^{-1}$ in terms of number of particles. Since all terms in Eq. (1) and Eq. (4) are linear with respect to the number concentration, results can be simply scaled to other value of the source intensity if needed.

Inlet wind profile is set as logarithmic with $u_{\mathrm{ref}} = 10\,\mathrm{m\,s}^{-1}$ at height 20 m and $z_0 = 0.1$ m. For the number concentration in the sectional model and for all moments in the moment method the Neumann boundary conditions are used on the ground, at the top and at the outlet. No resuspension of the particles is allowed, i.e. any particle that falls on the ground stays on the ground indefinitely. Small value of the concentration and of the moments calculated from the lognormal distribution with the parameters $N = 10^{-6}\mathrm{m}^{-3}, d_{gn} = 0.86\,\mu\mathrm{m}, \sigma_g = 2.21$ is prescribed at the inlet.

Domain is discretized using a cartesian grid with 220 cells in horizontal direction and 100 cells in vertical direction, graded so that the grid is finer near the ground and around the tree patch. The near ground cells are 0.25 m high, and the vegetation block itself consists of 42 x 40 cells.

Flow field obtained by the CFD solver is shown on Fig. 8. As visible, the

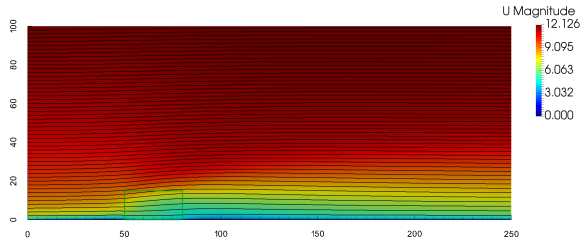

Figure 8: Flow field for the 2D tree patch case. Shown are the streamlines, background is coloured by velocity magnitude (in $\mathrm{m\,s}^{-1}$). Position of the tree patch is marked by a green rectangle.

vegetation block slows the wind down, but allows the air to pass through.

Results from the sectional and the moment model are compared in terms of the third moment of the particle size distribution, proportionate to the volume concentration of the particles. As we assume that the density is the same for particles of all sizes, third moment is also proportionate to the mass concentration of the particles.

Calculated field of the third moment by the moment method is shown on Fig. 9 (left). The relative difference $(M_3^{mm} - M_3^{sec})/M_3^{mm}$ of the results obtained by the moment method, M_3^{mm}, and by the sectional model, M_3^{sec}, is shown on the right panel of Fig. 9.

The source of the largest discrepancies between the two methods is the vegetation block. The relative difference raises up to 4% at the downstream edge of the vegetation block, and then decreases with the increasing distance from

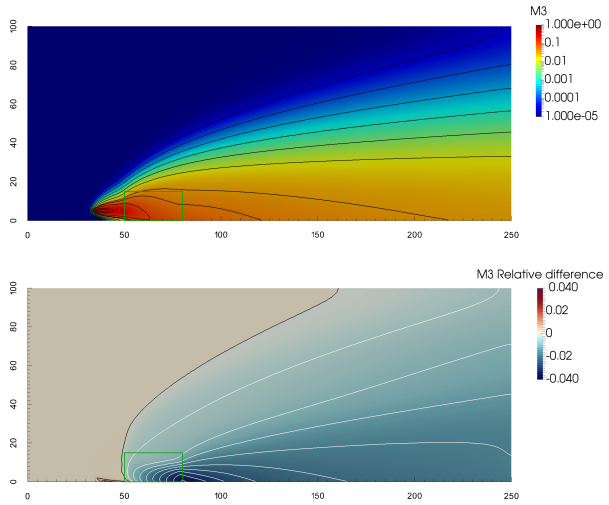

Figure 9: Results for the 2D tree patch case. (Top) Third moment of the size distribution calculated by the moment method (in $\mu m^3\ m^{-3}$). (Bottom) Relative difference $(M_3^{mm} - M_3^{sec})/M_3^{mm}$ of the third moment calculated by the moment method and the sectional approach.

the vegetation. The moment method overpredicts the deposition inside the vegetation due to the inexact approximation of the impaction efficiency described in section 2.3.3.

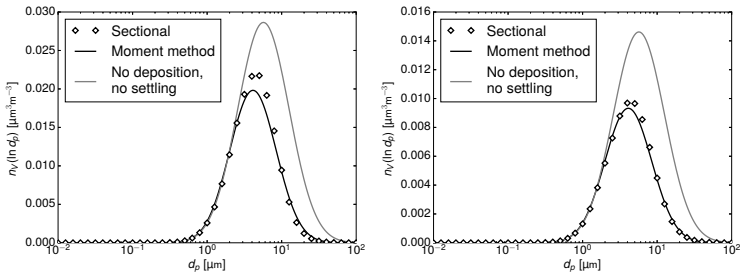

Figure 10: Results for the 2D tree patch case. (Left) Volume concentration at [80; 2] (Right) Volume concentration at [200; 2]. Discrete points calculated by the sectional method and the distribution calculated by the moment method are shown. For reference, the distribution calculated without the size dependent deposition and gravitational settling terms is shown as well.

Further insights can be obtained from Fig. 10. It shows the volume concentration distribution at the downstream edge of the tree patch, and at 120 m downstream from the tree patch, both at height 2 m above ground. The vegetation has negligible effect on the particles smaller than 2 µm, but significantly reduces the mass of the particles above 10 µm. This is captured well both by the

sectional and the moment method. At the downstream edge of the tree patch the moment method predicts lower peak of the volume concentration distribution than the sectional approach. The difference is reduced by the mixing of the filtered air with the unfiltered air flowing above the vegetation further away from the tree patch.

3.2. Hedgerow in 3D

Next we tested the method on a 3D model of a dense hedgerow placed near a line source of the pollutant. This case is a three dimensional extension of the 2D situation investigated in (Tiwary et al., 2005). The yew hedge is 10 m wide, 3.2 m deep and 2.4 m high. It is placed in the 40 m wide, 40 m long, and 20 m high computational domain. Two meters upstream from the hedge is a line source at height 0.5 m above ground. Intensity of the line source is set to a value $1\,\mathrm{s}^{-1}\,\mathrm{m}^{-1}$ in terms of number of particles, noting as in section 3.1 that the results can be scaled if other value is desired.

Sketch of the domain is shown on the left panel of Fig. 11. Right panel shows the LAD profile of the hedge, taken from the original article. Vegetation is further described by the needle diameter is, $d_e = 3\,\mathrm{mm}$, and the vegetation drag coefficient which is set to $C_d = 0.5$ as in (Tiwary et al., 2005).

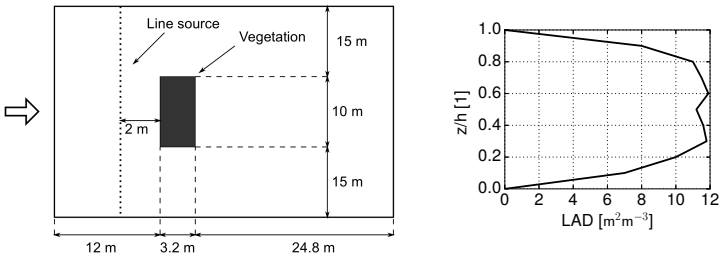

Figure 11: (Left) Overhead view of the domain (not to scale) (Right) LAD profile of the vegetation.

The computational mesh was created using the OpenFOAM *snappyHexMesh* generator. The domain consist of 376 000 cells, refined near the ground and around the hedge. The near-ground cells are 0.07 m high and the hedge itself is discretized using 54 x 20 x 22 cells.

Wind profile at the inlet is set as logarithmic with $u_{\mathrm{ref}} = 2.5\,\mathrm{m\,s}^{-1}$ at height 2.4 m and $z_0 = 0.1$ m. Boundary conditions for the sectional solver and moment method solvers are set similarly as in section 3.1: Neumann boundary conditions are used at the ground, top, sides, and at the outlet. No resuspension of the particles fallen to the ground is allowed. Again, small amount of the particles given by the lognormal distribution with the parameters $N = 10^{-6}, d_{gn} = 0.86\,\mu\mathrm{m}, \sigma_g = 2.21$ is prescribed at the inlet.

Streamlines of the flow field calculated by the separate CFD solver are shown on Fig. 12. As in the 2D simulation in (Tiwary et al., 2005), recirculation zone

is developed behind the dense hedge. Unlike the 2D case, here we can observe part the of the flow to be deflected to the sides.

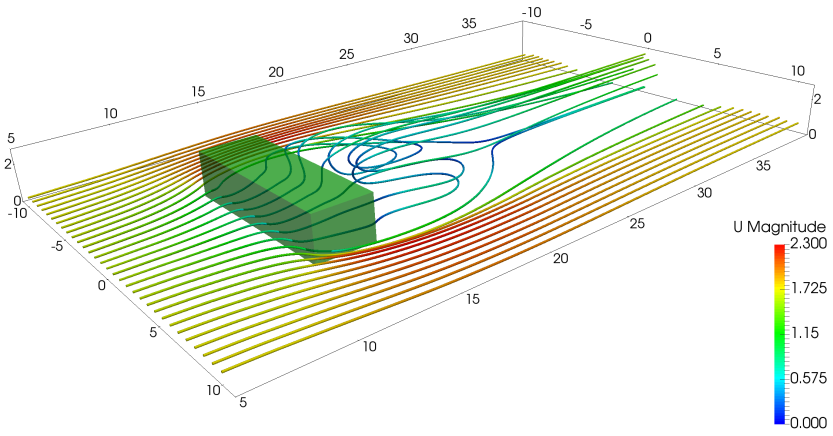

Figure 12: Streamlines of the flow around the hedgerow. Streamlines are released at height 0.5 m and are coloured by the velocity magnitude.

Third moment of the particle size distribution obtained by the moment method is shown on the left panels of Fig. 13 and Fig. 14. While a portion of the pollutant penetrates the barrier, part is deflected to the sides of the hedgerow, creating a zone with a reduced pollutant concentration behind it.

Relative difference between the solution obtained by the moment method and sectional approach is shown on the right panels of Fig. 13 and Fig. 14. As in the tree patch case, the moment method overpredicts the deposition and consequently underestimates the volume concentration behind the barrier. The difference is below 10%, and decreases away from the barrier.

Effects of the coarser mesh in the upper part of the computational domain are visible on Fig. 14. However, it does not negatively affect the difference between the two methods.

Volume concentration distribution at two points - inside the vegetation and downstream from the vegetation - is shown on Fig. 15. Due to the smaller size of the vegetation than in the 2D tree patch case, the effect of the vegetation is less pronounced. The moment method is able to reproduce the shape of the distribution well, but again produces a lower peak than the sectional method. Similarly as before, better fit can be observed further from the barrier due to the mixing with unfiltered air.

3.3. Computational performance

To compare the computational performance of the developed model, we measured the runtime of the sectional approach and the moment method approach

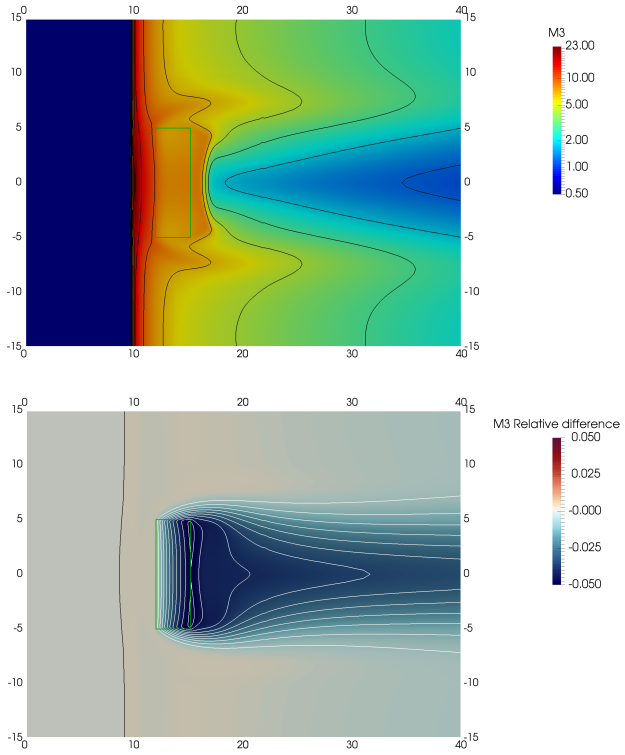

Figure 13: Results for the 3D hedgerow case. Horizontal cut at height $z = 0.5$ m. Quantities shown are as on Fig. 9.

for the 3D case described in section 3.2. Both solvers were run on a single core of an Intel Xeon X5365 processor.

The sectional model, comprised of 41 scalar PDEs, finished in 9120 seconds. The average runtime per each equation was thus 222 seconds. Moment model, comprised of 3 coupled PDEs, finished in 1128 seconds. That gives us eightfold acceleration compared to the sectional model. Even though the high number of bins used in this study might not be necessary to obtain sufficiently accurate results, to get an equivalent workload as the moment method in this case, only 5 bins could be used in the sectional model. Such number is insufficient to model the behaviour of the number distribution as well as the volume distribution well.

Two points can be made in favor of the sectional method though. First, the solution process of every equation is independent on the other equations, therefore the approach offers effortless parallelization for the number of cores up to the numbers of bins used. This is not especially advantageous in our implementation, as the OpenFOAM solvers are already parallelizable, but it could be an important factor for other implementations. Secondly, the relaxation factor 0.95 used for all simulations in the sectional approach was needed only for the

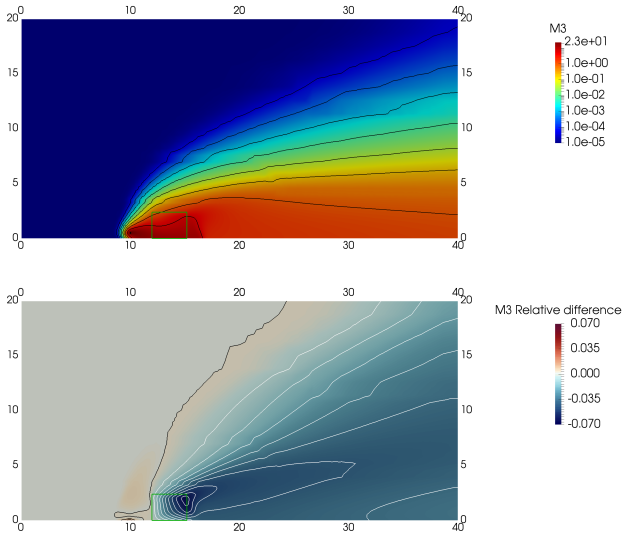

Figure 14: Results for the 3D hedgerow case. Vertical cut at $y = 0$ m. Quantities shown are as on Fig. 9.

bins representing the larger particles. Using different values of this parameter for different bins can provide some reduction of the runtime.

4. Conclusions

In this study, we introduced a formulation of a dry deposition model suitable for implementation in a moment method. As the original model by Petroff et al. (2008b), our approximation includes five main processes of the dry deposition: Brownian diffusion, interception, impaction, turbulent impaction, and sedimentation.

The developed deposition velocity model was implemented in a microscale finite volume solver based on the OpenFOAM platform. The solver employs the moment method to calculate the particle size distribution in the domain. The deposition model was tested on two example problems of microscale pollutant dispersion. Comparison with the sectional method using the original dry deposition model revealed that the moment method is able to reproduce the shape of the particle size distribution well. The relative differences between the sectional and the moment method in terms of the third moment of the distribution were below 10 %. This difference was caused by the higher deposition velocity in our model, which in turn was caused by the inexact representation of the impaction process. The impaction term could be represented better by employing numerical integration, that would however result in a higher computational costs, and reduce the advantages of using the moment method.

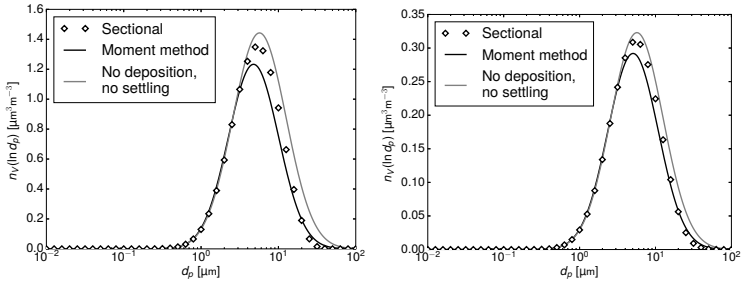

Figure 15: Results for the 3D hedgerow case. (Left) Volume concentration at [15; 0; 2]. (Right) Volume concentration at [30; 0; 2]. For reference, the distribution calculated without the size dependent deposition and gravitational settling terms is shown.

The moment method, described by three coupled PDEs, proved to be more computationally efficient than the sectional model using 41 bins. The speedup was approximately eightfold, and a workload equivalent to the moment method would be achieved by running a sectional model that uses only 5 bins.

This performance improvement together with the reliable results shows that the moment methods, often used in large scale atmospheric models, can be useful also for the microscale problems of pollutant dispersion in the urban environment.

The developed method as formulated here is applicable only when the particle size distribution can be approximated as a lognormal distribution. Here we used only unimodal distribution, but the usage of multimodal distribution would be also possible by superposition of several unimodal ones. Furthermore, the method could be reformulated for other distributions, provided that algebraic relations between the moments and distribution parameters are known.

Acknowledgements

This work was supported by the grant SGS16/206/OHK2/3T/12 of the Czech Technical University in Prague. Authors would like to thank to Jan Halama and Jiří Fürst for helpful discussions.

Nomenclature

$\boldsymbol{g}$	Gravity acceleration vector [ms^{-2}]
$\boldsymbol{u}$	Wind velocity [m s^{-1}]
$\boldsymbol{u}_s(d_p)$	Particle settling velocity [m s^{-1}]
λ	Mean free path of the particle in the air, λ= 0.066 µm
μ_a	Dynamic viscosity of the air [kg m^{-1} s^{-1}]

ν_a	Kinematic viscosity of the air [$\mathrm{m^2\ s^{-1}}$]
ν_T	Turbulent kinematic viscosity [$\mathrm{m^3\,s^{-1}}$]
ρ_a	Air density [$\mathrm{kg\ m^{-3}}$]
ρ_p	Particle density [$\mathrm{kg\ m^{-3}}$]
σ_g	Geometric standard deviation [1]
τ_p	Particle relaxation time, $\tau_p = (\rho_p C_C d_p^2)/(18\mu_a)$ [s]
τ_p^+	Dimensionless particle relaxation time, $\tau_p^+ = \tau_p u_f^2/\nu_a$
C_C	Cunningham correction factor [1]
D	Diffusion coefficient, $D = \nu_T/\mathrm{Sc}$ [$\mathrm{m^3\,s^{-1}}$]
D_B	Brownian diffusion coefficient, $D_B = (C_C k_b T_a)/(3\pi\mu_a d_p)$ [$\mathrm{m^2\ s^{-1}}$]
d_e	Needle diameter [m]
d_p	Particle diameter [m]
d_{gn}	Geometric mean size [m]
k_b	Boltzmann constant [$\mathrm{J\,K^{-1}}$]
M_k	k-th moment of the size distribution [$\mathrm{m^k\ m^{-3}}$]
$n(d_p)$	Number concentration of particles [$\mathrm{m^{-3}}$]
N	Total number concentration [$\mathrm{m^{-3}}$]
$n_V(d_p)$	Volume concentration of particles [$\mathrm{\mu m^3\ m^{-3}}$]
Re	Reynolds number, $Re = U d_e/\nu_a$ [1]
S	Total surface concentration [$\mathrm{\mu m^2\ m^{-3}}$]
Sc	Schmidt number, $Sc = \nu_a/D_B$ [1]
Sc_T	Turbulent Schmidt number [1]
St	Stokes number, $St = \tau_p U/d_e$ [1]
T_a	Temperature of the air [K]
U	Wind velocity magnitude [$\mathrm{m\,s^{-1}}$]
$u_d(d_p)$	Deposition velocity [$\mathrm{ms^{-1}}$]
u_f	Local friction velocity [$\mathrm{m\,s^{-1}}$]
V	Total volume concentration [$\mathrm{\mu m^3\ m^{-3}}$]
LAD	Leaf Area Density [$\mathrm{m^2\ m^{-3}}$]

References

Bae, S., Jung, C., Kim, Y., 2009. Development of an aerosol dynamics model for dry deposition process using the moment method. Aerosol Sci. Technol. 43 (6), 570–580.

Binkowski, F., Shankar, U., 1995. The regional particulate matter model: 1. model description and preliminary results. J. Geophys. Res. 100 (D12), 26191–26209.

Greenshields, C. J., 2015. OpenFOAM - The Open Source CFD Toolbox - User's Guide. Version 3.0.0. CFD Direct Ltd.

Gromke, C., Blocken, B., 2015a. Influence of avenue-trees on air quality at the urban neighborhood scale. Part I: Quality assurance studies and turbulent schmidt number analysis for RANS CFD simulations. Environ. Pollut. 196, 214–223.

Gromke, C., Blocken, B., 2015b. Influence of avenue-trees on air quality at the urban neighborhood scale. Part II: Traffic pollutant concentrations at pedestrian level. Environ. Pollut. 196, 176–184.

Hinds, W., 1999. Aerosol technology: Properties, Behavior, and Measurement of Airborne Particles, 2nd Edition. Wiley.

Janhäll, S., 2015. Review on urban vegetation and particle air pollution - deposition and dispersion. Atmos. Environ. 105, 130–137.

Jeanjean, A., Hinchliffe, G., McMullan, W., Monks, P., Leigh, R., 2015. A CFD study on the effectiveness of trees to disperse road traffic emissions at a city scale. Atmos. Environ. 120, 1–14.

Jung, C., Kim, Y., Lee, K., 2003. A moment model for simulating raindrop scavenging of aerosols. J. Aerosol Sci. 34 (9), 1217–1233.

Katul, G., Mahrt, L., Poggi, D., Sanz, C., 2004. One- and two-equation models for canopy turbulence. Bound. Layer Meteor. 113, 81–109.

Kenjereš, S., ter Kuile, B., 2013. Modelling and simulations of turbulent flows in urban areas with vegetation. J. Wind Eng. Ind. Aerodyn. 123, 43–55.

Koziol, A., Leighton, H., 2007. The moments method for multi-modal multi-component aerosols as applied to the coagulation-type equation. Q. J. R. Meteorol. Soc. 133 (625), 1057–1070.

Lalic, B., Mihailovic, D., Apr. 2004. An empirical relation describing leaf-area density inside the forest for environmental modeling. J. Appl. Meteor. 43, 641–645.

Litschke, T., Kuttler, W., 2008. On the reduction of urban particle concentration by vegetation - a review. Meteorol. Z. 17, 229–240.

Mochida, A., Lun, I. Y., 2008. Prediction of wind environment and thermal comfort at pedestrian level in urban area. J. Wind Eng. Ind. Aerodyn. 96 (10–11), 1498–1527, 4th International Symposium on Computational Wind Engineering (CWE2006).

Petroff, A., Mailliat, A., Amielh, M., Anselmet, F., 2008a. Aerosol dry deposition on vegetative canopies. Part I: Review of present knowledge. Atmos. Environ. 42, 3625–3653.

Petroff, A., Mailliat, A., Amielh, M., Anselmet, F., 2008b. Aerosol dry deposition on vegetative canopies. Part II: A new modelling approach and applications. Atmos. Environ. 42 (16), 3654–3683.

Petroff, A., Zhang, L., Pryor, S., Belot, Y., 2009. An extended dry deposition model for aerosols onto broadleaf canopies. J. Aerosol Sci. 40 (3), 218–240.

Pirjola, L., Kulmala, M., Wilck, M., Bischoff, A., Stratmann, F., Otto, E., 1999. Formation of sulphuric acid aerosols and cloud condensation nuclei: an expression for significant nucleation and model comparison. J. Aerosol Sci. 30 (8), 1079–1094.

Raupach, M., Briggs, P., Ford, P., Leys, J., Muschal, M., Cooper, B., Edge, V., 2001a. Endosulfan transport ii. modeling airborne dispersal and deposition by spray and vapor. J. Environ. Qual. 30 (3), 729–740.

Raupach, M., Woods, N., Dorr, G., Leys, J., Cleugh, H., 2001b. The entrapment of particles by windbreaks. Atmos. Environ. 35, 3373–3383.

Richards, P., Hoxey, R., 1993. Appropriate boundary conditions for computational wind engineering models using the k-ϵ turbulence model. J. Wind Eng. Ind. Aerodyn. 46 & 47, 145–153.

Seinfeld, J., Pandis, S., 2006. Atmospheric Chemistry and Physics: From Air Pollution to Climate Change, 2nd Edition. A Wiley-Interscience publication. Wiley.

Steffens, J., Wang, Y., Zhang, K., 2012. Exploration of effects of a vegetation barrier on particle size distributions in a near-road environment. Atmos. Environ. 50, 120–128.

Tiwary, A., Morvanb, H., Colls, J., 2005. Modelling the size-dependent collection efficiency of hedgerows for ambient aerosols. J. Aerosol Sci. 37, 990–1015.

Tominaga, Y., Stathopoulos, T., 2007. Turbulent Schmidt numbers for CFD analysis with various types of flowfield. Atmos. Environ. 41, 8091–8099.

Vranckx, S., Vos, P., Maiheu, B., Janssen, S., 2015. Impact of trees on pollutant dispersion in street canyons: A numerical study of the annual average effects in Antwerp, Belgium. Sci. Total Environ. 532, 474–483.

Whitby, E., McMurry, P., 1997. Modal aerosol dynamics modeling. Aerosol Sci. Technol. 27 (6), 673–688.

Whitby, E., McMurry, P., Shankar, U., Binkowski, F., 1991. Modal aerosol dynamics modeling. Tech. rep., U.S. Environmental Protection Agency, Research Triangle Park, NC 27711.

Šíp, V., Beneš, L., 2016. CFD optimization of a vegetation barrier. In: Karasözen, B., Manguoglu, M., Tezer-Sezgin, M., Göktepe, S., Ömür Ugur (Eds.), Numerical Mathematics and Advanced Applications - ENUMATH 2015. Springer International Publishing, Cham, to appear.